Macromolecules
ARTICLE

Macromolecules **2009**, *42*, 9515–9522 **9515**
DOI: 10.1021/ma901964a

Interactive Crystallization of a Strongly Segregated Double Crystalline Block Copolymer with Close Crystallizable Temperatures

Shuichi Nojima,* Yoshimasa Fukagawa, and Hiroshi Ikeda

Department of Organic and Polymeric Materials, Graduate School of Science and Engineering, Tokyo Institute of Technology, H-125, 2-12-1 Ookayama, Meguro-Ku, Tokyo 152-8552, Japan

Received June 13, 2009; Revised Manuscript Received November 9, 2009

ABSTRACT: The crystallization process of a new crystalline−crystalline diblock copolymer with close crystallizable temperatures, poly(β-propiolactone)-*block*-linear low density polyethylene (PPL-*b*-PE), has been investigated using differential scanning calorimetry (DSC), synchrotron small-angle X-ray scattering (SR-SAXS), and Fourier transform infrared spectroscopy (FTIR). PPL-*b*-PE formed a strongly segregated microdomain structure in the melt, so that crystallization of both PPL and PE blocks was effectively confined within this structure without morphological transition. When PPL-*b*-PE was cooled from the microphase-separated melt at constant rates (*i.e.*, nonisothermal crystallization), the PE block started to crystallize first, followed immediately by the crystallization of PPL blocks. As a result, the crystallization process of PPL blocks was overlapped with the late stage of PE crystallization (coincident crystallization), where crystallization of one block significantly affected the crystallization behavior of the other block. When PPL-*b*-PE was isothermally crystallized, such coincident crystallization was not observed and both blocks crystallized separately.

1. Introduction

Morphology formation occurring in crystalline−crystalline diblock copolymers is extremely complicated due to the interplay between two kinds of crystallization starting from the microphase-separated melt.[1,2] Several diblock copolymers have been used to investigate such morphology formation, where the crystallizable temperatures of two blocks, T_{c1} and T_{c2}, are important to understand the crystallization process and eventually to control the morphology formed in the system.

When $T_{c1} \gg T_{c2}$, the block 1 with T_{c1} crystallizes first by quenching or gradually cooling the copolymer from the melt into low temperatures, where crystallization destroys the existing microdomain structure to form the *crystallized lamellar morphology* if two blocks are weakly segregated in the melt. Subsequently, the block 2 with T_{c2} starts to crystallize from the crystallized lamellar morphology. This crystallization behavior has been reported so far on polyethylene-*block*-poly(ethylene oxide) (PE-*b*-PEO),[3−5] poly(L-lactide)-*block*-PEO (PLLA-*b*-PEO),[6−11] PLLA-*block*-poly(ε-caprolactone) (PLLA-*b*-PCL),[7,12−15] and PE-*b*-PCL.[16−19] For example, we have recently investigated the morphology formation of PE-*b*-PCL, and showed that the PE block crystallized first to form the PE-crystallized lamellar morphology followed by PCL crystallization, where the resulting morphology depended significantly on the copolymer composition, total molecular weight, and crystallization temperature.

When $T_{c1} \sim T_{c2}$, we have the possibility of observing coincident crystallization of both blocks when the copolymer is quenched or cooled from the melt, and therefore a unique crystallization behavior is expected. PEO-*b*-PCL diblock copolymers have been frequently used to investigate the coincident crystallization behavior.[20−30] Shiomi et al.[23] and He et al.,[26] for example, reported the formation of interesting spherulites consisting of PCL cores and PEO coronas, which was ascribed to the difference in crystallization rates between PEO and PCL blocks. However, the electron density of amorphous PEO blocks (354 e/nm^3 at 80 °C) is nearly the same to that of amorphous PCL blocks (342 e/nm^3 at 80 °C), so that the small-angle X-ray scattering (SAXS) method does not provide information on the phase state of PEO-*b*-PCL before crystallization (*i.e.*, miscible or microphase-separated). Therefore, the effects of existing microdomain structures on crystallization cannot be clarified only from the SAXS results.

Recently, Myers and Register investigated the morphology formation of weakly segregated hydrogenated polynorbornene-*block*-polyethylene (hPNB-*b*-PE) diblocks with close crystallizable temperatures.[31] They found the crystallization mechanism was intimately dependent on the composition and crystallization temperature. Coincident crystallization was also observed in weakly segregated poly(*p*-dioxanone)-*block*-PCL (PPDX-*b*-PCL)[32,33] and strongly segregated PLLA-*b*-PE.[34,35] Though the crystallizable temperature of one block (PPDX or PLLA) was significantly higher than that of the other, coincident crystallization was observed because the crystallization rate of higher-T_c blocks was considerably retarded owing to the presence of lower-T_c blocks.

In this study, the crystallization process of a strongly segregated poly(β-propiolactone)-*block*-linear low density polyethylene (or hydrogenated polybutadiene) (PPL-*b*-PE) copolymer is investigated using differential scanning calorimetry (DSC), synchrotron small-angle X-ray scattering (SR-SAXS), and Fourier transform infrared spectroscopy (FTIR). This copolymer is interesting in that the crystallizable temperature of PE blocks can be designed by changing the branching ratio, that is, by controlling the synthesis condition of PE blocks (Scheme 1). We synthesized two PPL-*b*-PE copolymers, for which the crystallizable temperature of PE blocks was moderately close to that of PPL blocks (Figure 4). The PPL and PE blocks were strongly segregated in the melt and the microdomain structure was completely preserved after crystallization (confined

*Corresponding author. Telephone:+81-3-5734-2132. Fax:+81-3-5734-2888. E-mail snojima@polymer.titech.ac.jp.

Published on Web 11/23/2009

Scheme 1. Synthesis Route of PPL-*b*-PE

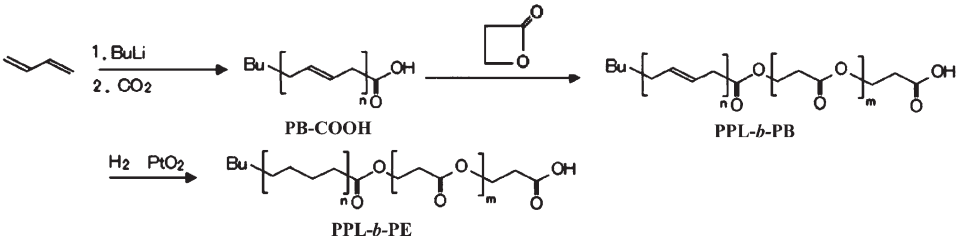

Table 1. Molecular Characteristics of Samples Used in This Study

sample code	M_n of PPL blocks[a] (g/mol)	M_n of PE (or PB) blocks[a] (g/mol)	mol % of 1−2 linkage[a]	total M_n	M_w/M_n[b]	PPL:PE (or PB) (wt %)	PPL:PE (or PB) (vol % at 100 °C)
PPL−PB1	6100	4800	10	10 900	1.15	56:44	46:54
PPL−PB2	8300	4800	10	13 100	1.17	63:37	54:46
PPL−PE1	6100	5000	10	11 100	1.15	55:45	45:55
PPL−PE2	8300	5000	10	13 300	1.17	62:38	52:48
PE[c]		4700			1.05	0:100	0:100

[a] Determined by ^{1}H NMR. [b] Determined by GPC. [c] Obtained from Polymer Laboratory Inc.

crystallization), that is, the PPL and PE blocks crystallized within it to form the *crystallized microdomain structure*.

2. Experimental Section

2.1. Samples. The crystalline−crystalline diblock copolymer used in this study is poly(β-propiolactone)-*block*-linear low density polyethylene (or hydrogenated polybutadiene) (PPL-*b*-PE). The synthesis route is briefly shown in Scheme 1. The butadiene monomer in toluene was first polymerized at room temperature for 24 h with *n*-buthyllithium as an initiator and the reaction was terminated by adding carbon dioxide to obtain carboxyl-terminated polybutadiene (PB-COOH). Next, β-propiolactone in tetrahydrofuran (THF) was polymerized at 40 °C for 24−48 h with PB-COOH as the initiator. The reaction was stopped by adding a large amount of acetic acid to obtain PPL-*b*-PB. Finally, PPL-*b*-PB in THF was hydrogenated with PtO_2 at 5 MPa and 70 °C for 1 week. The PPL-*b*-PE copolymer was purified several times by precipitating the hot THF solution into methanol to remove the impurities included. The molecular weight (M_n) and composition were evaluated using ^{1}H NMR, and the polydispersity (M_w/M_n) was obtained using gel permeation chromatography (GPC) with polystyrene standards.

We synthesized two PPL-*b*-PE copolymers. Table 1 shows the molecular characteristics of PPL-*b*-PE, together with PPL-*b*-PB (precursor of PPL-*b*-PE before hydrogenation) and PE homopolymer. The total molecular weight of PPL-*b*-PE is 11,100−13,300 and the volume fraction of PPL blocks is around 0.5, and therefore the lamellar microdomain structure is expected in the melt for both copolymers. All the experiments described below were mainly performed with PPL−PE2, and PPL−PE1 was supplementarily used in this study. The PPL block showed thermal degradation at high temperatures (≥120 °C); *i.e.*, the molecular weight changed gradually, so that the copolymers were treated at temperatures under 120 °C in every experiment.

Following specific volumes were used to calculate the volume fraction of each block from ^{1}H NMR results. For amorphous PPL[36]

$$v_{sp}(T) = 0.7209 + (6.0 \times 10^{-4}) \times T \quad (1)$$

and for amorphous PE[37]

$$v_{sp}(T) = 1.1696 + (1.77 \times 10^{-4}) \times T \quad (2)$$

where $v_{sp}(T)$ is in cubic centimeter per gram and T is in degrees Celsius.

2.2. Wide-Angle X-ray Diffraction (WAXD). Two-dimensional WAXD (2D-WAXD) measurements were performed using a Rigaku conventional equipment with a rotating-anode X-ray generator operating at 45 kV and 60 mA. The wavelength used was 0.1542 nm of Cu Kα radiation. The detector was an image plate (FUJI Film BAS-SR 127) with the size of 10 cm × 10 cm. The accumulation time for each measurement was 30 min. After subtracting the background scattering, the 2D-WAXD pattern was circularly averaged to convert it into one-dimensional diffraction pattern, and finally the diffraction intensity was plotted against the diffraction angle 2θ.

2.3. Synchrotron Small-Angle X-ray Scattering (SR-SAXS). The morphology at each temperature was investigated using (static) synchrotron small-angle X-ray scattering (SR-SAXS). The crystallization process during cooling was also observed using (time-resolved) SR-SAXS. SR-SAXS measurements were performed at Photon Factory in High Energy Acceleration Research Organization, Tsukuba Japan, with a small-angle X-ray equipment for solution (SAXES) installed at beamline BL-10C. Details of the equipment and the instrumentation are described elsewhere.[38,39] The scattered intensity was detected with a one-dimensional position-sensitive proportional counter (PSPC) with the accumulation time of 300 s for the static measurement and 10 s for the time-resolved measurement. The SR-SAXS curves obtained were corrected for the background scattering and the absorption by the sample, but not for the smearing effect because SAXES employed the point-focusing optics. The SAXS curves were finally obtained as a function of wavenumber s defined as $s = (2/\lambda) \sin \theta$, where 2θ is the scattering angle and λ is the wavelength used (= 0.1488 nm).

2.4. Transmission Electron Microscope (TEM). The morphology after crystallization was observed using TEM (JEOL model 200CX with an acceleration voltage of 100 kV). The bulk sample crystallized at 50 °C was exposed to RuO_4 vapor at room temperature for 24 h to give the contrast and also to fix the morphology, then microtomed at room temperature into a sliver with ca. 60 nm in thickness, and finally the sliver was again exposed to RuO_4 vapor for 1 h at room temperature. RuO_4 diffuses easily into the amorphous region of PPL and PE blocks to present dark contrast, whereas the PPL and PE crystals show bright contrast owing to slow diffusion of RuO_4.[40] Therefore, when the lamellar morphology of amorphous and crystallized layers is formed in the system, it can be confirmed by an alternating structure composed of dark (or amorphous) and bright (or crystallized) layers.

2.5. Differential Scanning Calorimetry (DSC). A Perkin-Elmer DSC Pyris 1 was used to observe the crystallization

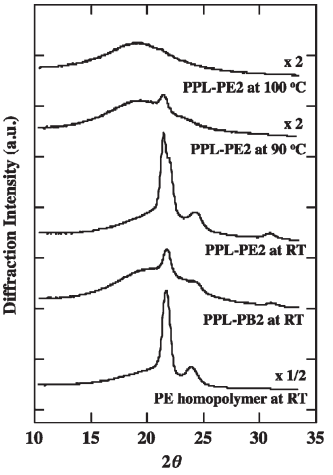

Figure 1. WAXD curves for the PE homopolymer and PPL−PB2 (corresponding to PPL homopolymer) at room temperature and PPL−PE2 at selected temperatures indicated. The WAXD curve for PPL−PE2 at 100 °C has the amorphous halo with no diffraction peak, indicating that PE blocks as well as PPL blocks are completely melted at 100 °C.

behavior during cooling at constant rates. We employed several cooling rates ranging from −10 to −1 °C/min, and the crystallinity of PE and PPL blocks, $\chi_{PE}(t)$ and $\chi_{PPL}(t)$, was calculated from the exothermic peak area as a function of time t during cooling when both DSC peaks were adequately separated. We assumed that the exothermic heat of crystallization to form perfect PE and PPL crystals was 277 J/g[41] and 119 J/g,[36] respectively.

2.6. Fourier Transform Infrared Spectroscopy (FTIR). FTIR spectra were recorded during cooling using JASCO FT-IR 6200 spectrometer with a spectral resolution of 4 cm^{-1}, and the normalized crystallinities of PE and PPL blocks, $\chi^*_{PE}(t)$ ($=\chi_{PE}(t)/\chi_{PE}(t_f)$) and $\chi^*_{PPL}(t)$ ($=\chi_{PPL}(t)/\chi_{PPL}(t_f)$), were evaluated as a function of t, where t_f represents the time when the sample arrives at the final temperature (~30 °C). The sample was first dissolved in chloroform, and thin films (ca. 100 μm in thickness) were prepared by the solution-casting method on a silicone plate. The absorption bands at 730 cm^{-1} for PE blocks and 1734 cm^{-1} for PPL blocks were mainly analyzed to evaluate the time evolution of $\chi^*_{PE}(t)$ and $\chi^*_{PPL}(t)$ during cooling, where the band at 730 cm^{-1} arises from CH_2 rocking motion in PE crystals[42] and that at 1734 cm^{-1} from C=O stretching motion in PPL crystals.[43] The isothermal crystallization process of PPL blocks was also evaluated from the t dependence of $\chi^*_{PPL}(t)$ for PPL-*b*-PE and PPL-*b*-PB.

3. Results and Discussion

3.1. Morphology before and after Crystallization. First, we confirm that the PE blocks (and also PPL blocks) are completely melted at 100 °C, from which we start to decrease the temperature to crystallize both the blocks. Figure 1 shows the WAXD curves for the PE homopolymer and PPL−PB2 (corresponding to PPL homopolymers) at room temperature (RT) and PPL−PE2 at selected temperatures indicated. The WAXD curve for PPL−PE2 at 100 °C (top curve in Figure 1) has a diffuse amorphous halo with no diffraction peak arising from PE crystals (bottom)[44] and PPL crystals (second from the bottom),[45,46] indicating that PE blocks as well as PPL blocks are completely melted at 100 °C. At 90 °C, only PE blocks crystallize partially and we can see a small diffraction arising from PE crystals (second from the top). In addition, we find that the WAXD curve for PPL−PE2 at room temperature (third from the top) is a combination of those for PPL and PE crystals,

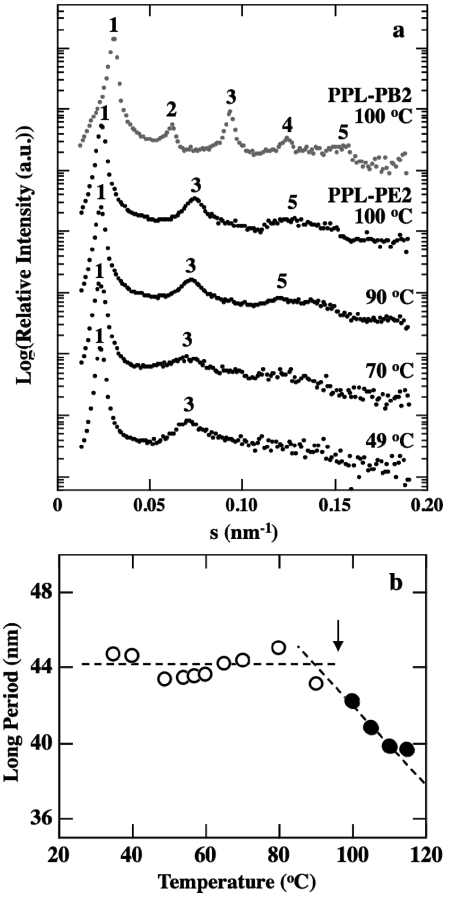

Figure 2. (a) Lorenz-corrected SR-SAXS curves for the molten PPL−PB2 at 100 °C (gray curve) and for PPL−PE2 at selected temperatures indicated. (b) The long period, evaluated from the SR-SAXS peak position, plotted against temperature for PPL−PE2. The closed circle represents the results from the molten PPL−PE2 and open circle from the PE- or PE + PPL-crystallized PPL−PE2.

indicating that both blocks certainly crystallize at low temperatures.

Figure 2a shows the Lorentz-corrected SAXS curves for PPL−PB2 at 100 °C (i.e., microphase-separated melt, gray curve) and PPL−PE2 at selected temperatures indicated (black curves). The SAXS curve from the molten PPL−PB2 has several scattering peaks, the angular positions of which exactly correspond to a ratio of 1:2:3:4:5, indicating that the lamellar microdomain structure is formed in the melt. The SAXS curve for PPL−PE2 at 100 °C arises from the melt, that at 90 °C from the PE-crystallized system, and those at 70 and 49 °C from the PE + PPL-crystallized system, which all have a couple of scattering peaks. The angular positions of these peaks correspond to a ratio of 1:3:(5), suggesting that the lamellar morphology is also formed in PPL−PE2 at each temperature. The absence of even-order peaks in the SAXS curves of PPL−PE2 is ascribed to the fact that the volume fraction of PPL blocks (~0.52) in PPL−PE2 is very close to 0.5 (Table 1).

Figure 2b shows the long period (LP), evaluated from the primary peak position, plotted against temperature for PPL−PE2, where the closed circles represent the results of the molten PPL−PE2 and open circles those of the crystallized PPL−PE2. LP of the molten microdomain structure increases steadily with decreasing temperature, which arises from the change in block incompatibility and chain conformation with changing temperature.[47] However, LP does not change significantly after crystallization (*i.e.*, $T \leq 90$ °C) and

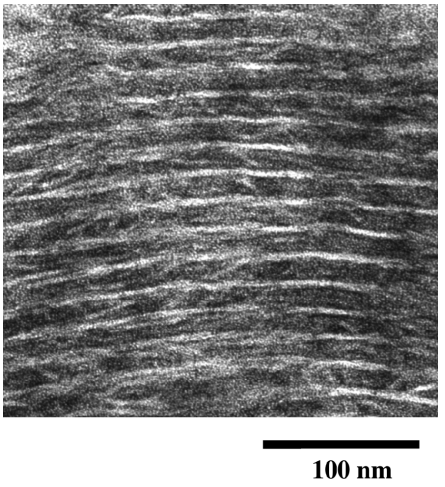

Figure 3. The TEM picture of PPL−PE2 crystallized at 50 °C.

is nearly equal to that of the molten microdomain structure existing just before crystallization (shown by an arrow), suggesting that the morphology is frozen by crystallization.

Figure 2b clearly indicates that the lamellar microdomain structure is completely preserved after crystallization. This is because if the morphological transition (molten microdomain structure → crystallized lamellar morphology) takes place by crystallization, LP changes discontinuously before and after crystallization.[48] Therefore, PPL and PE blocks are expected to crystallize within the existing microdomain structure to form the crystallized microdomain structure. This confined crystallization will be ascribed to the strong segregation between PE and PPL blocks judging from the considerably large LP (∼42.2 nm at 100 °C) for the low molecular weight copolymer (∼13 300). The strong segregation is also reported on PLLA-*b*-PE,[35] where the microdomain structure has an extremely large LP (∼75−78 nm for PLLA-*b*-PE with $M_n \sim 22\,500$). Both PLLA and PPL belong to the family of aliphatic polyesters and the molecular structure is very similar, so that it is reasonable that our PPL-*b*-PE copolymers form the strongly segregated microdomain structure in the melt.

Figure 3 shows the TEM picture of PPL−PE2 crystallized at 50 °C. We can find an alternating structure consisting of dark and bright layers, which correspond to amorphous PPL or PE layers and crystallized PPL or PE layers, respectively. The alternating period evaluated from Figure 3 is ca. 20 nm and almost the half of LP evaluated from SAXS results (∼44.1 nm in Figure 2b). The TEM picture reflects the alternating structure of crystallized and amorphous layers irrespective of the constituent blocks, and therefore the TEM period should be the half of LP because the volume fraction of PPL layers (∼0.52) is nearly equal to that of PE layers in PPL−PE2.

In summary, PPL-*b*-PE forms the molten lamellar microdomain at 100 °C and the strong segregation between constituent blocks in PPL-*b*-PE yields confined crystallization below 100 °C. Consequently, PPL and PE blocks crystallize within the existing lamellar microdomain structure. Note that the sample was transparent after crystallization of both blocks because of confined crystallization, and we could not observe the superstructure (such as spherulite structure) using an optical microscope.

3.2. Crystallization Process during Cooling at Constant Rates. The crystallization process of PPL-*b*-PE during cooling at constant rates was investigated using DSC and SR-SAXS. Figure 4 shows the typical DSC curves of PPL−PE2

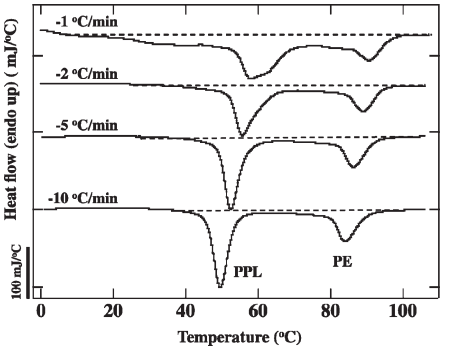

Figure 4. Typical DSC curves for PPL−PE2 obtained at various cooling rates indicated.

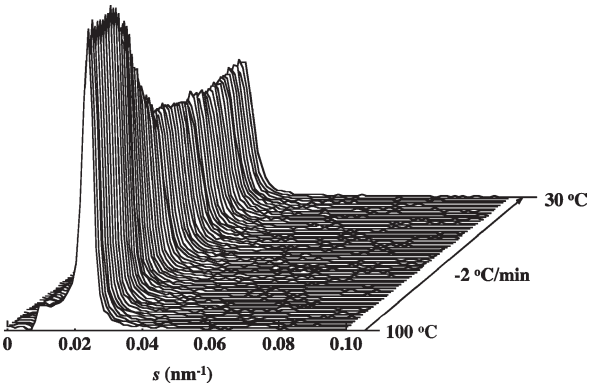

Figure 5. Time-resolved SR-SAXS curves of PPL−PE2 during cooling at −2 °C/min from 100 °C (molten state) into 30 °C.

at various cooling rates indicated, where the crystallization of PE blocks occurs at 80−95 °C (depending on cooling rates) followed by PPL crystallization at 45−70 °C. When the cooling rate is larger (−5 ∼ −10 °C/min), two kinds of crystallization seem to be independent, that is, PPL crystallization starts after completion of PE crystallization. However, the tail of the PE exothermic peak overlaps with the initial stage of PPL crystallization at smaller cooling rates (≤−2 °C/min). In particular, the DSC curve at −1 °C/min shows a continuous exothermic heat flow between two crystallization peaks, which consists of the combination of two exothermic curves owing to PE and PPL crystallization. The overlap of two crystallization processes is mainly ascribed to the extended temperature range of PE crystallization, which is well-known to be characteristic of low density PE. Therefore, coincident crystallization is strongly expected in the limited temperature range during cooling at −2 °C/min or less.

The typical time-resolved SR-SAXS curves of PPL−PE2 during cooling at −2 °C/min are shown in Figure 5. At 100 °C, the primary scattering peak, together with the small higher-order peaks (not detected in the normal plot), arises from the molten lamellar microdomain structure. The peak intensity decreases significantly when the PE block crystallizes, because the electron density of PE crystals (340 e/nm^3 [37]), rather than amorphous PE (290 e/nm^3 at 100 °C[37]), is closer to that of amorphous PPL (410 e/nm^3 at 100 °C[36]). Subsequently, the peak intensity keeps almost constant owing to the increase of electron density in both lamellae by the formation of PE and PPL crystals (460 e/nm^3 [36]) during coincident crystallization. It is important to point out that the angular position of the primary peak does not change significantly over the whole cooling process, which leads to the same conclusion derived from

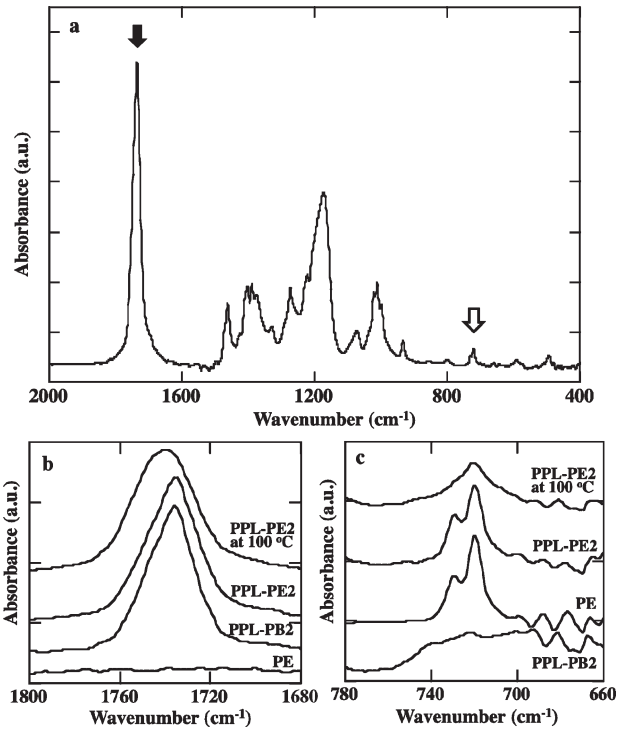

Figure 6. (a) FTIR curve of PPL−PE2 at 30 °C. (b and c) Detailed FTIR curves of PPL−PE2 at 100 °C and PPL−PE2, PPL−PB2, and PE homopolymers at 30 °C for the selected ranges of wavenumber.

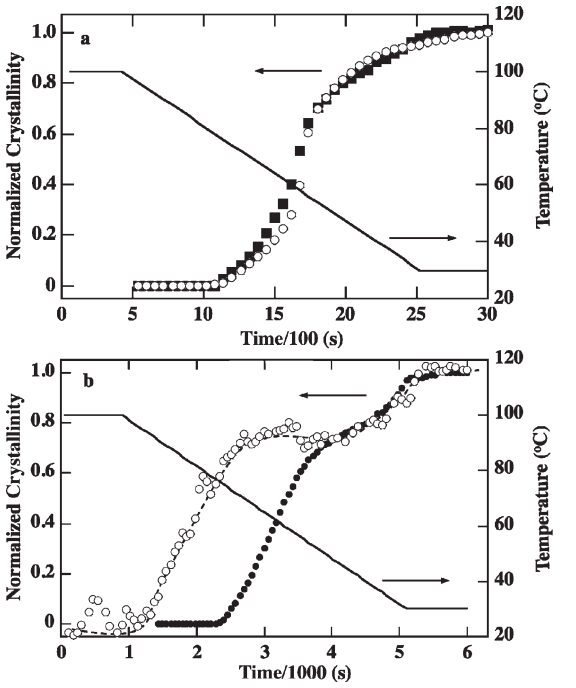

Figure 7. (a) Normalized crystallinity of PPL blocks in PPL−PB2, obtained using DSC (open circles) and FTIR (closed squares), plotted against time during cooling at −2 °C/min from 100 °C into 30 °C (right ordinate). (b) Normalized crystallinity of PPL blocks (closed circle) and PE blocks (open circle) in PPL−PE2, obtained using FTIR, plotted against time during cooling at −1 °C/min from 100 °C into 30 °C.

Figures 2 and 3. That is, Figure 5 clearly indicates that the PE and PPL blocks crystallize within the existing lamellar microdomain structure (confined crystallization), and the morphological transition does not take place by the crystallization of constituent blocks.

3.3. FTIR Analysis of Nonisothermal Crystallization during Cooling. Figure 6a shows the typical FTIR curve of PPL−PE2 at 30 °C, and Figures 6b and 6c are the detailed curves of PPL−PE2 at 100 °C (*i.e.*, microphase-separated melt) and PPL−PE2, PPL−PB2, and PE homopolymer at 30 °C (PE and PPL-crystallized state) in the wavenumber range used for the analysis of the crystallization process for PPL (b) and PE (c) blocks. That is, we evaluated $\chi^*_{PPL}(t)$ from the absorption band at 1734 cm^{-1} (indicated by the black arrow in Figure 6a) as a function of t during cooling, and independently $\chi^*_{PE}(t)$ from the band at 730 cm^{-1} (the white arrow), as described in Experimental Section.

Figure 7a shows the time dependence of $\chi^*_{PPL}(t)$ evaluated from FTIR results of PPL−PB2 during cooling at −2 °C/min from 100 °C into 30 °C (closed square), where only PPL blocks crystallize within the lamellar microdomain structure. Therefore, it is also possible to independently evaluate $\chi^*_{PPL}(t)$ from the DSC exothermic peak area arising from PPL crystallization (open circles in Figure 7a). Though the crystallization process of PPL blocks is nonisothermal, $\chi^*_{PPL}(t)$ increases sigmoidally, which is usually observed in the isothermal crystallization process of homopolymers. The important result shown in Figure 7a is that the time dependence of $\chi^*_{PPL}(t)$ obtained from FTIR results is almost identical to that from DSC results. That is, the crystallization process is successfully evaluated from FTIR measurements, and we can investigate the crystallization process of PPL and PE blocks in PPL-*b*-PE using FTIR. On the other hand, the DSC method can not be used to evaluate $\chi^*_{PPL}(t)$ and $\chi^*_{PE}(t)$ separately for PPL-*b*-PE, because the exothermic peak of PE blocks partially overlaps with that of PPL blocks for the crystallization process of PPL-*b*-PE under slower cooling rates (Figure 4).

The time dependence of $\chi^*_{PPL}(t)$ and $\chi^*_{PE}(t)$ for PPL−PE2 during cooling at −1 °C/min from 100 to 30 °C is shown in Figure 7b, where the data points of $\chi^*_{PE}(t)$ are moderately scattered because the absorption band at 730 cm^{-1} for evaluating $\chi^*_{PE}(t)$ is considerably small compared to that at 1734 cm^{-1} for $\chi^*_{PPL}(t)$ (Figure 6a). The crystallization of PE blocks starts at $t \sim 1150$ s (∼98 °C) and $\chi^*_{PE}(t)$ increases steadily with increasing t. The PPL blocks, on the other hand, start to crystallize at $t \sim 2400$ s (∼76 °C), where $\chi^*_{PE}(t)$ is still increasing, and hence, we can observe a coincident crystallization process after $t \geq 2400$ s (or $T \leq 76$ °C). The new finding shown in Figure 7b is that the time dependence of $\chi^*_{PE}(t)$ and $\chi^*_{PPL}(t)$ is not represented by a sigmoidal curve, as observed for PPL−PB2 (Figure 7a) and many crystalline homopolymers, but the crystallization rate of both blocks changes complicatedly during coincident crystallization. That is, the crystallization of PPL blocks significantly affects the crystallization process of PE blocks, and vice versa. It should be noted that $\chi^*_{PE}(t)$ and $\chi^*_{PPL}(t)$ do not change anymore at $t \sim 5000$ s (∼30 °C), which might be related to the fact that the cooling process finishes at 30 °C.

3.4. Interrelation between Two Crystallization Processes. Though the nonisothermal crystallization process of polymers is very important in industrial applications, it is extremely complicated from the viewpoint of basic science because the nucleation and growth rates change significantly depending on temperature during cooling. Therefore, the comprehensive theories describing the whole process of nonisothermal crystallization are not available. Here, we phenomenologically investigate the effect of crystallization of one block on the crystallization behavior of the other block during cooling. For this purpose, we compare the

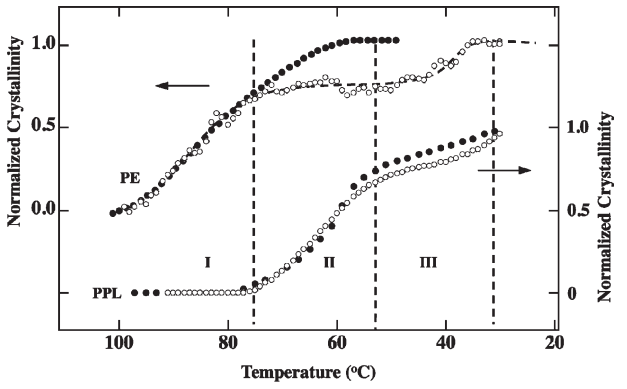

Figure 8. (Top) Normalized crystallinity of PE homopolymers (closed circle) and PE blocks in PPL−PE2 plotted against temperature during cooling. (Bottom) Normalized crystallinity of PPL blocks in PPL−PB2 (closed circle) and PPL blocks in PPL−PE2 (open circle) plotted against temperature.

temperature dependence of the normalized crystallinity for each block (PPL and PE blocks in PPL−PE2) with that of corresponding chains without coincident crystallization (PPL block in PPL−PB2 and PE homopolymer).

Figure 8 shows the normalized PE and PPL crystallinities (Figure 7b) replotted against temperature. It also includes the temperature dependence of the normalized crystallinities for PE homopolymers and PPL blocks in PPL−PB2 (corresponding to PPL homopolymers), which have no effect of another crystallization. It should be noted that the normalized crystallinity of PE homopolymers is shifted horizontally so as to overlap with that of PE blocks at the early stage of crystallization ($T \geq 90$ °C). It is usually observed that the crystallizable temperature of crystalline blocks is moderately lower than that of corresponding homopolymers owing to the tethering effect of amorphous blocks.[49]

In the temperature region I (95 °C $\geq T \geq$ 76 °C), where only PE blocks crystallize and PPL blocks remain amorphous, the existing PPL blocks do not practically affect the crystallization of PE blocks, resulting in the similar temperature dependence of the crystallinity for PE blocks and PE homopolymers. At $T \sim 76$ °C, the PPL block starts to crystallize and then the PPL crystallinity increases extremely with decreasing temperature (temperature region II), where the crystallization rate of PE blocks considerably decelerates and the crystallinity soon falls constant. Therefore, the difference in crystallinity between PE blocks and PE homopolymers increases notably with decreasing temperature. The crystallinity increase of PE blocks is expected to arise mainly from the growth of PE crystals in the temperature region II because it is the late stage of crystallization for PE blocks, whereas the nucleation process will control the crystallinity development of PPL blocks at the beginning of the region II followed by the growth process of PPL crystals. Figure 8 suggests that the nucleation process of PPL blocks overwhelms the growth process of PE blocks at the beginning of the region II, which makes deceleration of PE crystal growth, resulting in the almost constant PE crystallinity during the region II. In the temperature region III, the growth of PPL crystals is the major process for the crystallization process of PPL blocks, which will have the comparable driving force with the growth process of PE crystals. As a result, we have the cooperative growth of both crystals in the region III, where we can find that the crystallinity growth of PPL blocks in PPL−PE2 is slower than that of PPL blocks in PPL−PB2.

The PE and PPL blocks are completely confined within each constituent layer of the microdomain structure during the whole process of crystallization, and therefore both blocks do not directly interact except at the interfacial region between two layers. In addition, the interfacial thickness is expected to be extremely thin owing to the strong segregation between PE and PPL blocks. Therefore, the interactive crystallization processes observed in Figure 7b will work through the junction point between both blocks located at the interfacial region. That is, the accelerating crystallization (or nucleation) of PPL blocks yields the conformational stress of the amorphous part of PPL blocks, which will be relaxed by deforming the interface and/or by moving the junction point through the interface.[50] This conformational relaxation will be the additional stress for the amorphous part of PE blocks, resulting in the decelerating crystallization (or crystal growth) of PE blocks. Similar interacting crystallization behavior, i.e., crystallization-induced melting, has been recently reported for some crystalline−crystalline diblocks with $T_{c1} > T_{c2}$.[14,18] However, this crystallization behavior is considered to arise from the melting of block 1 facilitated by further crystallization of block 2 in order to compensate the space previously occupied by the amorphous block 2. Therefore, the interactive crystallization behavior observed in this study is substantially different from the crystallization-induced melting process, and can be expected only for coincident crystallization in crystalline−crystalline diblocks with close crystallizable temperatures.

In summary, two crystallization processes interact intimately with each other during the coincident crystallization process of both blocks, where crystallization of one block significantly affects the crystallization behavior of the other block through the junction point between two blocks.

3.5. FTIR Analysis of Isothermal Crystallization. Finally, we report the results of isothermal crystallization of PPL-*b*-PE. When PPL-*b*-PE was quenched from the microphase-separated melt (~100 °C) into the crystallization temperature T_c (55 $\leq T_c \leq$ 70 °C), the PE block always crystallized first during quenching followed by the crystallization of PPL blocks, and no coincident crystallization was observed. Figure 9a shows the time evolution of $\chi_{PPL}(t)$ derived from FTIR measurements for PPL−PB2 (closed circle) and for PPL−PE2 (open circle) both crystallized at 65 °C. The time dependence of $\chi_{PPL}(t)$ for PPL−PB2 shows a sigmoidal curve with some induction time, which is usually observed in isothermal crystallization of homopolymers. This crystallization behavior is also in good agreement with the results reported on many strongly segregated crystalline−amorphous diblock copolymers with soft lamellar microdomains[50−52] and suggests that the spatial confinement by the amorphous layers (PB layers in the present case) is not perfect but some defects exist in the orientation of lamellar microdomains to yield the heterogeneous nucleation.

The time evolution of $\chi_{PPL}(t)$ for PPL−PE2, on the other hand, is extremely different from that for PPL−PB2. In particular, the difference is remarkable at the initial stage of crystallization, where the crystallization of PPL blocks in PPL−PE2 starts just after quenching ($t \sim 0$ s) with no induction time. The crystallinity increases steeply at the beginning of crystallization and then reaches asymptotically to the final value (~0.40), which is significantly smaller than that of PPL−PB2 (~0.58). The crystallization process of PPL blocks in PPL−PE2 is similar to that observed for the crystalline blocks confined in isolated microdomain structures (*i.e.*, spheres and cylinders),[53,54] where the spatial confinement is virtually perfect and eventually the crystallization behavior is understood by the first-order kinetics,

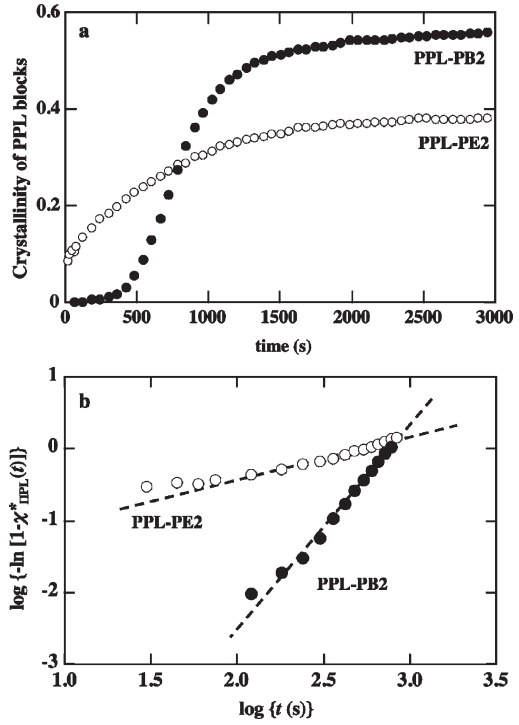

Figure 9. (a) Crystallinity of PPL blocks in PPL−PE2 (open circle) and PPL−PB2 (closed circle) plotted against crystallization time when the samples were isothermally crystallized at 65 °C. (b) Avrami plot based on the crystallinity development for PPL−PE2 (open circle) and PPL−PB2 (closed circle).

i.e., the rate of isothermal crystallization is simply proportional to the fraction of uncrystallized domains existing in the system at t.

The early stage of crystallization of PPL blocks in PPL−PB2 and PPL−PE2 was analyzed using the Avrami equation, which is widely used for the analysis of crystallization mechanism of bulk homopolymers.[55] The normalized crystallinity $\chi^*_{PPL}(t)$ at t is given by,

$$\chi^*_{PPL}(t) = 1 - \exp[-(Kt)^n] \quad (3)$$

where K is a rate constant and n is the Avrami index expressing the mode of crystallization. It is possible to evaluate n and K from the plot of log $\{-\ln [1 - \chi^*_{PPL}(t)]\}$ against log t. Figure 9b shows the result of the Avrami plot for the crystallization process of PPL blocks in PPL−PE2 (open circle) and PPL−PB2 (closed circle). The value of n, evaluated from the slope in Figure 9b is ca. 2.7 for PPL−PB2 and 0.6−0.9 for PPL−PE2 depending on the fitting range we used. The significant difference in n between two systems indicates that the crystallization mechanism is completely different between them.

The crystallization behavior of block chains confined within the lamellar microdomain structure has been investigated for some crystalline−amorphous diblock copolymers.[50−52] The glassy (or hard) lamellar microdomain structure usually confines crystallization within it to yield the first-order kinetics, whereas the amorphous (or soft) microdomain structure results in the sigmoidal crystallization kinetics with the appreciable deformation of the structure.[50] The difference between our PPL−PB2 and PPL−PE2 systems is only that when the PPL block starts to crystallize within PPL layers of lamellar microdomains, the other constituent layer (PB or PE layer) is amorphous or already crystallized. Therefore, from the viewpoint of the crystallization kinetics of PPL blocks, the PE-crystallized lamellar microdomain structure works as the hard microdomain to successfully confine PPL crystallization, resulting in the first-order kinetics. It is speculated that this result might be ascribed to the fact that the PPL lamellae, sandwiched by the PE-crystallized layers, have less defects (or interconnection between two PPL lamellae) and the spatial confinement is more effective compared to the case of usual soft lamellar microdomains.

In summary, when PPL-*b*-PE was isothermally crystallized, coincident crystallization could not be observed, and the PE blocks always crystallized first during quenching followed by the crystallization of PPL blocks. The crystallization behavior of PPL blocks in PPL-*b*-PE was significantly different from that in PPL-*b*-PB. That is, the Avrami index was 0.6−0.9 for PPL-*b*-PE while it was 2.7 for PPL-*b*-PB.

Conclusion

The interactive crystallization process of a new crystalline−crystalline diblock copolymer with close crystallizable temperatures, poly(β-propiolactone)-*block*-linear low density polyethylene (PPL-*b*-PE), has been investigated using DSC, SR-SAXS, and FTIR. PPL-*b*-PE formed the strongly segregated microdomain structure in the melt, so that crystallization of both blocks was effectively confined within this structure without any morphological transition. When PPL-*b*-PE was cooled from the melt at constant rates (*i.e.*, nonisothermal crystallization), the PE blocks crystallized first followed immediately by PPL crystallization, where the crystallization of PPL blocks was overlapped with the late stage of PE crystallization (coincident crystallization). The time dependence of $\chi^*_{PPL}(t)$ and $\chi^*_{PE}(t)$ was found to be very complicated during coincident crystallization. That is, crystallization of one block significantly affected the crystallization behavior of the other block, resulting in the characteristic change in the crystallization rate of both blocks.

On isothermal crystallization of PPL-*b*-PE, the PE blocks crystallized first during quenching and subsequently the PPL blocks crystallized, where the interactive crystallization processes was not observed. However, the crystallization behavior of PPL blocks, starting from the PE-crystallized microdomain structure, was significantly different from that of PPL blocks in PPL-*b*-PB.

Acknowledgment. We acknowledge with appreciation Mr. J. Koki, Center for Advanced Materials Analysis, Tokyo Institute of Technology, for TEM observations. The SR-SAXS measurement has been performed under the approval of the Photon Factory Advisory Committee (No. 2008G031).

References and Notes

(1) Muller, A. J.; Arnal, M. L.; Balsamo, V. *Progress in Understanding of Polymer Crystallization*; Reiter, G., Strobl, G. R., Eds.; Lecture Notes in Physics 714; Springer: Berlin, 2007.
(2) Castillo, R. V.; Muller, A. J. *Prog. Polym. Sci.* **2009**, *34*, 516.
(3) Sun, L.; Liu, Y.; Zhu, L.; Hsiao, B. S.; Avila-Orta, C. A. *Polymer* **2004**, *45*, 8181.
(4) Castillo, R. V.; Arnal, M. L.; Muller, A. J.; Hamley, I. W.; Castelletto, V.; Schmalz, H.; Abetz, V. *Macromolecules* **2008**, *41*, 879.
(5) Cao, W.; Tashiro, K.; Hanesaka, M.; Takeda, S.; Masunaga, H.; Sasaki, S.; Takata, M. *J. Phys. Chem. B* **2009**, *113*, 2338.
(6) Kim, K. S.; Chung, S.; Chin, I. J.; Kim, M. N.; Yoon, J. S. *J. Appl. Polym. Sci.* **1999**, *72*, 341.
(7) Maglio, G.; Migliozzi, A.; Palumbo, R. *Polymer* **2003**, *44*, 369.
(8) Sun, J.; Hong, Z.; Yang, L.; Tang, Z.; Chen, X.; Jing, X. *Polymer* **2004**, *45*, 5969.
(9) Yang, J.; Zhao, T.; Cui, J.; Liu, L.; Zhou, Y.; Li, G.; Zhou, E.; Chen, X. *J. Polym. Sci.* **2006**, *B44*, 3215.

(10) Yang, J.; Zhao, T.; Liu, L.; Zhou, Y.; Li, G.; Zhou, E.; Chen, X. *Polym. J.* **2006**, *38*, 1251.
(11) Huang, S.; Jiang, S.; An, L.; Chen, X. *J. Polym. Sci.* **2008**, *B46*, 1400.
(12) Kim, J. K.; Park, D. J.; Lee, M. S.; Ihn, K. J. *Polymer* **2001**, *42*, 7429.
(13) Ho, R. M.; Hsieh, P. Y.; Tseng, W. H.; Lin, C. C.; Huang, B. H.; Lotz, B. *Macromolecules* **2003**, *36*, 9085.
(14) Hamley, I. W.; Castelletto, V.; Castillo, R. V.; Muller, A. J.; Martin, C. M.; Pollet, E.; Dubois, P. *Macromolecules* **2005**, *38*, 463.
(15) Hamley, I. W.; Parras, P.; Castelletto, V.; Castillo, R. V.; Muller, A. J.; Pollet, E.; Dubois, P.; Martin, C. M. *Macromol. Chem. Phys.* **2006**, *207*, 941.
(16) Nojima, S.; Akutsu, Y.; Washino, A.; Tanimoto, S. *Polymer* **2004**, *45*, 7317.
(17) Nojima, S.; Akutsu, Y.; Akaba, M.; Tanimoto, S. *Polymer* **2005**, *46*, 4060.
(18) Nojima, S.; Ito, K.; Ikeda, H. *Polymer* **2007**, *48*, 3607.
(19) Sakurai, T.; Ohguma, Y.; Nojima, S. *Polym. J.* **2008**, *40*, 971.
(20) Nojima, S.; Ono, M.; Ashida, T. *Polym. J.* **1992**, *24*, 1271.
(21) Gan, Z.; Jiang, B.; Zhang, J. *J. Appl. Polym. Sci.* **1996**, *59*, 961.
(22) Bogdanov, B.; Vidts, A.; Schacht, E.; Berghmans, H. *Macromolecules* **1999**, *32*, 726.
(23) Shiomi, T.; Imai, K.; Takenaka, K.; Takeshita, H.; Hayashi, H.; Tezuka, Y. *Polymer* **2001**, *42*, 3233.
(24) Jiang, S.; He, C.; An, L.; Chen, X.; Jiang, B. *Macromol. Chem. Phys.* **2004**, *205*, 2229.
(25) Ghoroghchian, P. P.; Li, G.; Levine, D. H.; Davis, K. P.; Bates, F. S.; Hammer, D. A.; Therien, M. J. *Macromolecules* **2006**, *39*, 1673.
(26) He, C.; Sun, J.; Zhao, T.; Hong, Z.; Zhuang, X.; Chen, X.; Jing, X. *Biomacromolecules* **2006**, *7*, 252.
(27) Sun, J.; Chen, X.; He, C.; Jing, X. *Macromolecules* **2006**, *39*, 3717.
(28) Takeshita, H.; Fukumoto, K.; Ohnishi, T.; Ohkubo, T.; Miya, M.; Takenaka, K.; Shiomi, T. *Polymer* **2006**, *47*, 8210.
(29) Du, Z. X.; Yang, Y.; Xu, J. T.; Fan, Z. Q. *J. Appl. Polym. Sci.* **2007**, *104*, 2986.
(30) Li, L.; Meng, F.; Zhong, Z.; Byelov, D.; De-Jeu, W. H.; Feijen, J. *J. Chem. Phys.* **2007**, *126*, 024904.
(31) Myers, S. B.; Register, R. A. *Macromolecules* **2008**, *41*, 6773.
(32) Albuerne, J.; Marquez, L.; Muller, A. J.; Raquez, J. M.; Degee, P.; Dubois, P.; Castelletto, V.; Hamley, I. W. *Macromolecules* **2003**, *36*, 1633.
(33) Muller, A. J.; Albuerne, J.; Marquez, L.; Raquez, J. M.; Degee, P.; Dubois, P.; Hobbs, J.; Hamley, I. W. *Faraday Discuss, Chem. Soc.* **2005**, *128*, 231.
(34) Muller, A. J.; Castillo, R. V.; Hillmyer, M. *Macromol. Symp.* **2006**, *242*, 174.
(35) Castillo, R. V.; Muller, A. J.; Lin, M. C.; Chen, H. L.; Jeng, U. S.; Hillmyer, M. A. *Macromolecules* **2008**, *41*, 6154.
(36) Crescenzi, V.; Manzini, G.; Calzolari, G.; Borri, C. *Eur. Polym. J.* **1972**, *8*, 449.
(37) Stehling, F. C.; Mandelkern, L. *Macromolecules* **1970**, *3*, 242.
(38) Nojima, S.; Hashizume, K.; Rohadi, A.; Sasaki, S. *Polymer* **1997**, *38*, 2711.
(39) Nojima, S.; Kiji, T.; Ohguma, Y. *Macromolecules* **2007**, *40*, 7566.
(40) Trent, J. S.; Scheinbeim, J. I.; Couchman, P. R. *Macromolecules* **1983**, *16*, 589.
(41) Brandrup, J., Immergut, E. H., Eds, *Polymer Handbook*, 3rd ed.; John Wiley and Sons: New York, 1989.
(42) Hagemann, H.; Snyder, R. G.; Peacock, A. J.; Mandelkern, L. *Macromolecules* **1989**, *22*, 3600.
(43) Furuhashi, Y.; Iwata, T.; Kimura, Y.; Doi, Y. *Macromol. Biosci.* **2003**, *3*, 462.
(44) Swan, P. R. *J. Polym. Sci.* **1962**, *56*, 409.
(45) Wasai, T.; Saegusa, T.; Furukawa, J. *J. Chem. Soc. Jpn., Ind. Chem. Sect.*, **1964**, *67*, 601 (in Japanese).
(46) Suehiro, K.; Chatani, Y.; Tadokoro, H. *Polym. J.* **1975**, *7*, 352.
(47) Sakamoto, N.; Hashimoto, T. *Macromolecules* **1995**, *28*, 6825.
(48) Ikeda, H.; Ohguma, Y.; Nojima, S. *Polym. J.* **2008**, *40*, 241.
(49) Nandan, B.; Hsu, J. Y.; Chen, H. L. *J. Macromol. Sci., Part C, Polym. Rev.* **2006**, *46*, 143.
(50) Ho, R. M.; Lin, F. H.; Tsai, C. C.; Lin, C. C.; Ko, B. T.; Hsiao, B. S.; Sics, I. *Macromolecules* **2004**, *37*, 5985.
(51) Zhu, L.; Huang, P.; Chen, W. Y.; Ge, Q.; Quirk, R. P.; Cheng, S. D. Z.; Thomas, E. L.; Lotz, B.; Hsiao, B. S.; Yeh, F.; Liu, L. *Macromolecules* **2002**, *35*, 3553.
(52) Sun, Y. S.; Chung, T. M.; Li, Y. J.; Ho, R. M.; Ko, B. T.; Jeng, U. S.; Lotz, B. *Macromolecules* **2006**, *39*, 5782.
(53) Loo, Y. L.; Register, R. A.; Ryan, A. J. *Phys. Rev. Lett.* **2000**, *84*, 4120.
(54) Nojima, S.; Toei, M.; Hara, S.; Tanimoto, S.; Sasaki, S. *Polymer* **2002**, *43*, 4087.
(55) Avrami, M. J. *J. Chem. Phys.* **1939**, *7*, 1103.